MIGRATION OF RADIAL TRACE SECTIONS

Rick Ottolini

Introduction

A ***radial trace*** is a trace extracted approximately diagonally from a common midpoint gather. The motivation for migrating radial trace sections is that the double square root equation is simplified into a single square root imaging theory. The advantage of a single square root equation is that its migration and diffraction impulse responses are always smooth curves, unlike those of constant offset sections. Its migration is therefore easier to implement than the migration of constant offset sections or pre-stack dip compensation (Devilish). In fact, the constant velocity operator is the same as that for zero-offset sections except for a rescaling of the depth axis. Radial trace sections are also easier to construct than slant stacks, avoiding end-of-cable artifacts. However, the economic cost is similar to other migration-before-stack schemes. The main disadvantage is that the radial trace migration theory is exact only for constant velocity media or depth-variable velocity media and non-zero-dip sections.

Diffraction Curves on Radial Trace Sections

We begin with the double square root expression describing the point scatterer diffraction surface in midpoint-offset (y,h)–space as determined by Clayton (SEP-14):

$$vt = \left[z^2 + \left(y + h\right)^2\right]^{\frac{1}{2}} + \left[z^2 + \left(y - h\right)^2\right]^{\frac{1}{2}} \qquad (1)$$

For a point scatterer at location ($z=z_0, y=0$) equation (1) renders the rounded-pyramidal surface shown in figure 1. Cross sections of constant offset (fixed h) are contoured. These constant offset diffraction curves are hyperbolic at low offsets and have flattened tops at large offsets ($h > z$).

Constant offset migration schemes (Clayton, SEP-14; Rocca and Deregowski, SEP-16) and partial pre-stack migration (Yilmaz, SEP-18) have been unsuccessful in imaging such wide-offset diffractions. However, a simple substitution remaps midpoint-offset space into a space in which diffraction curves are always hyperbola-like. Offset is replaced by a function of time

$$h = rt \qquad (2)$$

where r is a parameter with dimensions of velocity that will be derived later. Equation (2) maps a diagonal line across a common midpoint gather beginning at the origin, which is called the radial trace. The cross section of the point scatterer diffraction surface described by equation (2) is shown in figure 2. From figure 2 it can be visualized that a plane emerging at any angle from zero time and zero offset and intersecting the diffraction surface will have a hyperbola-like cross section through the diffraction surface. This may be mathematically demonstrated by replacing h in equation (1) by equation (2) and solving for vt.

$$vt = 2\left[\frac{z^2}{\left(1 - \frac{4r^2}{v^2}\right)} + y^2\right]^{\frac{1}{2}} \qquad (3)$$

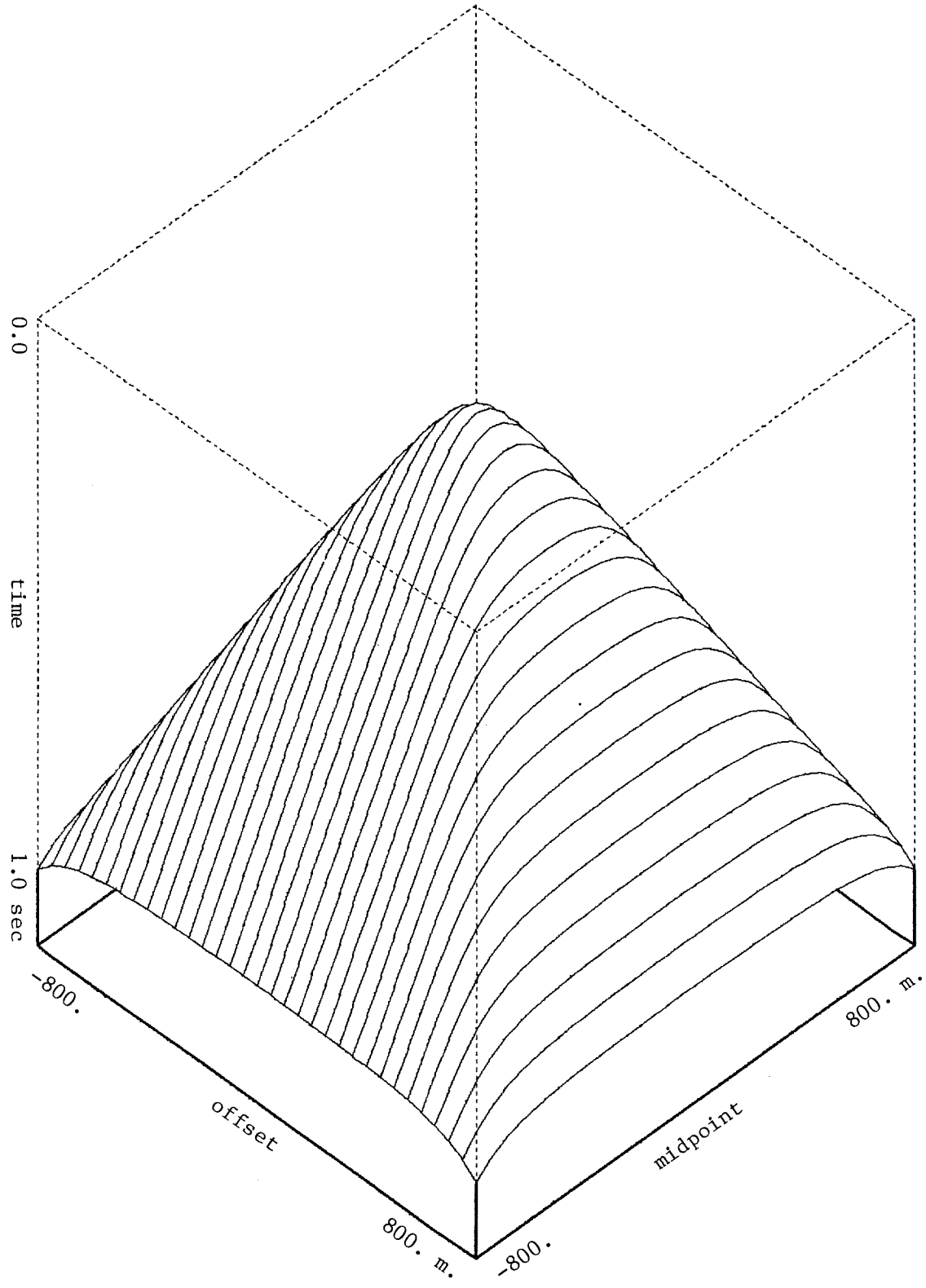

FIG. 1. Point scatterer diffraction surface in midpoint offset space as predicted by equation (1). Point scatterer located at y=0, h=0, z=150 m with constant media velocity of 2000 m/sec. Shape of the diffraction surface is pyramidal with rounded corners and peak. Contour lines are at constant offset with spacing of 50 m. At small offsets the constant offset cross section is hyperbola-like while at large offsets the cross section has a flattened top.

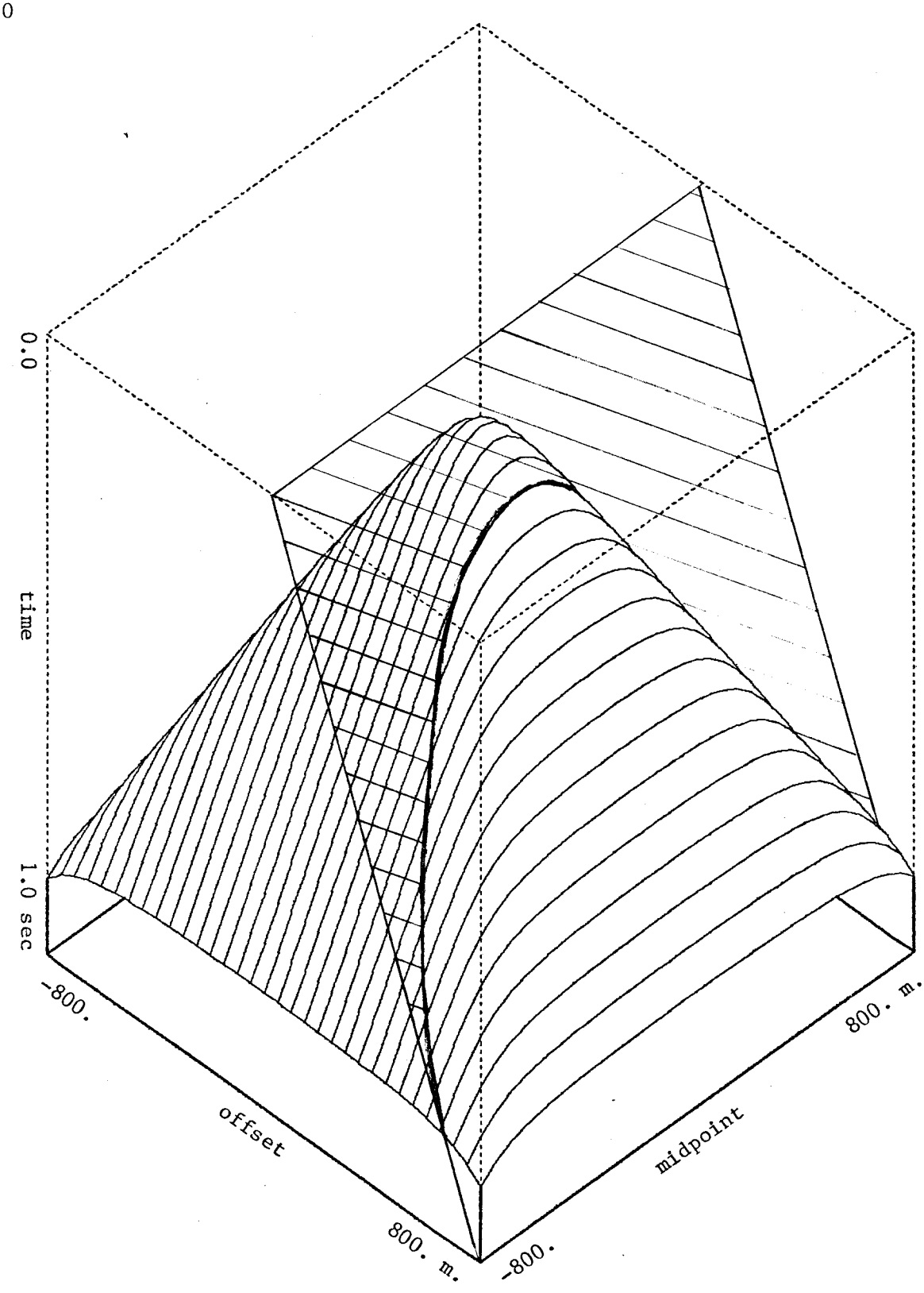

FIG. 2. The radial trace cross section through the same point scatterer cross section as in figure 1. In contrast to constant offset sections, the cross section diffraction curve is always hyperbola-like. One edge of the radial plane is fixed at h=t=0. The radial plane is flat for a constant velocity media. In this case the radial parameter r is 800 m/sec and its Snell parameter is p = 4.e-04.

Equation (3) describes a suite of hyperbolas with peaks displaced along the depth axis according to the radial parameter r with limbs all asymptotic at late arrival times. This suite of curves is depicted in figure 3. Thus constant velocity radial trace sections may be migrated with the zero-offset single square root operator and the resulting depth axis rescaled by

$$\left(1 - \frac{4r^2}{v^2}\right)^{\frac{1}{2}}$$

in order to produce a zero-offset earth image.

Derivation of the Radial Parameter r

Defining the ***radial parameter*** r in terms of the Snell parameter p gives a lead into the variable velocity situation, because p is a constant parameter of wave propagation in variable velocity media. Specifically, the radial trace is plotted through the set of tangencies between lines with a slope equal to Snell's parameter and hyperbolic reflection events on a common midpoint gather. Figure 4 illustrates this concept. Lines with Snell parameter slopes are of interest because summing the traces of the gather along this trajectory selects the plane wave components of the reflections which have propagated with this Snell parameter. These sums are called slant stack traces, for which a variable velocity migration theory is known. It will be shown there is a relationship between the reflection times of a radial and slant stack trace - hence the possibility of migrating variable velocity radial traces.

In order to determine the radial parameter of equation (2), expressions will be found for the radial trace time t_r, radial trace offset h_r, and slant time t_s from the geometry of figure 4. The hyperbolic equation of a reflection event is

$$v^2 t_h^2 = v^2 t_0^2 + 4h^2 \qquad (4)$$

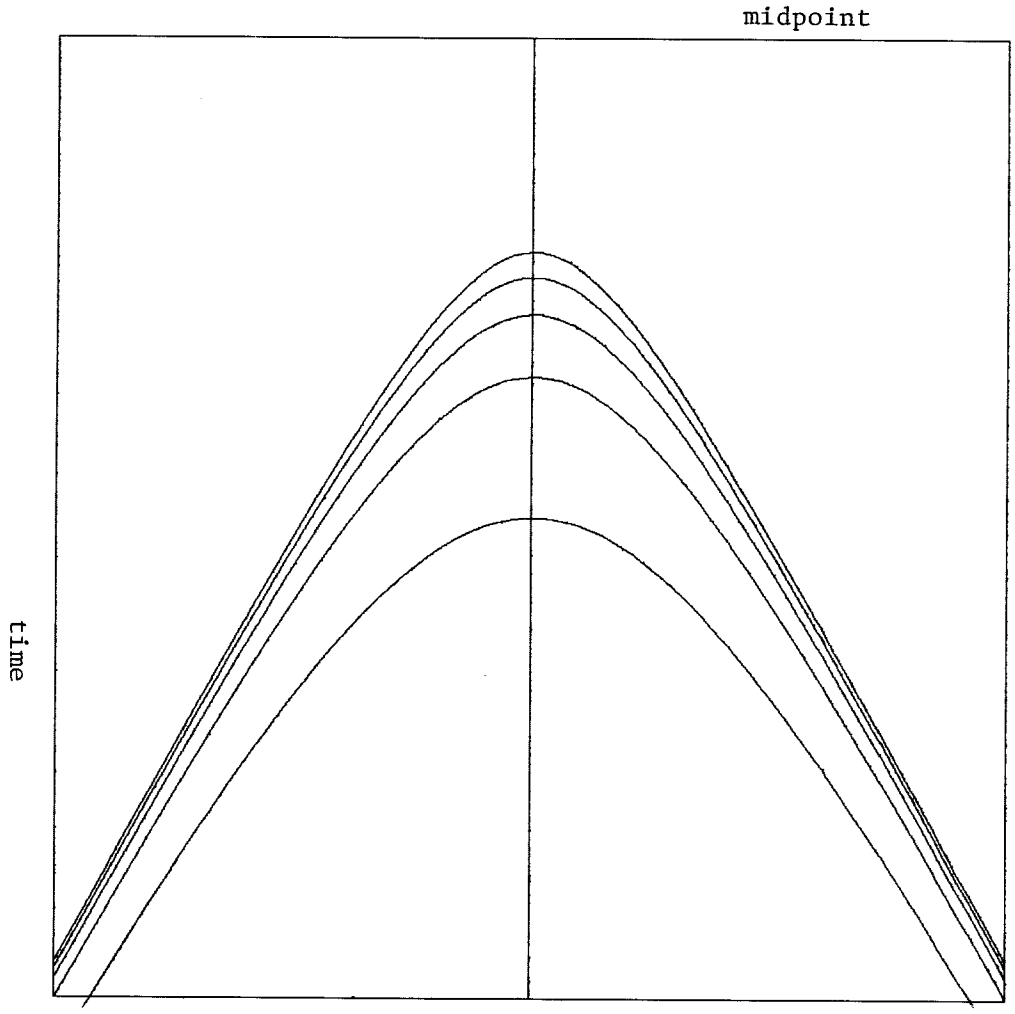

FIG. 3. Suite of radial trace diffraction hyperbolas for different radial parameters. The point scatterer is located at the peak of the uppermost curve. As the radial parameter is increased from zero, the peak of each hyperbola is displaced further down the time axis. At large time all the limbs are asymptotic.

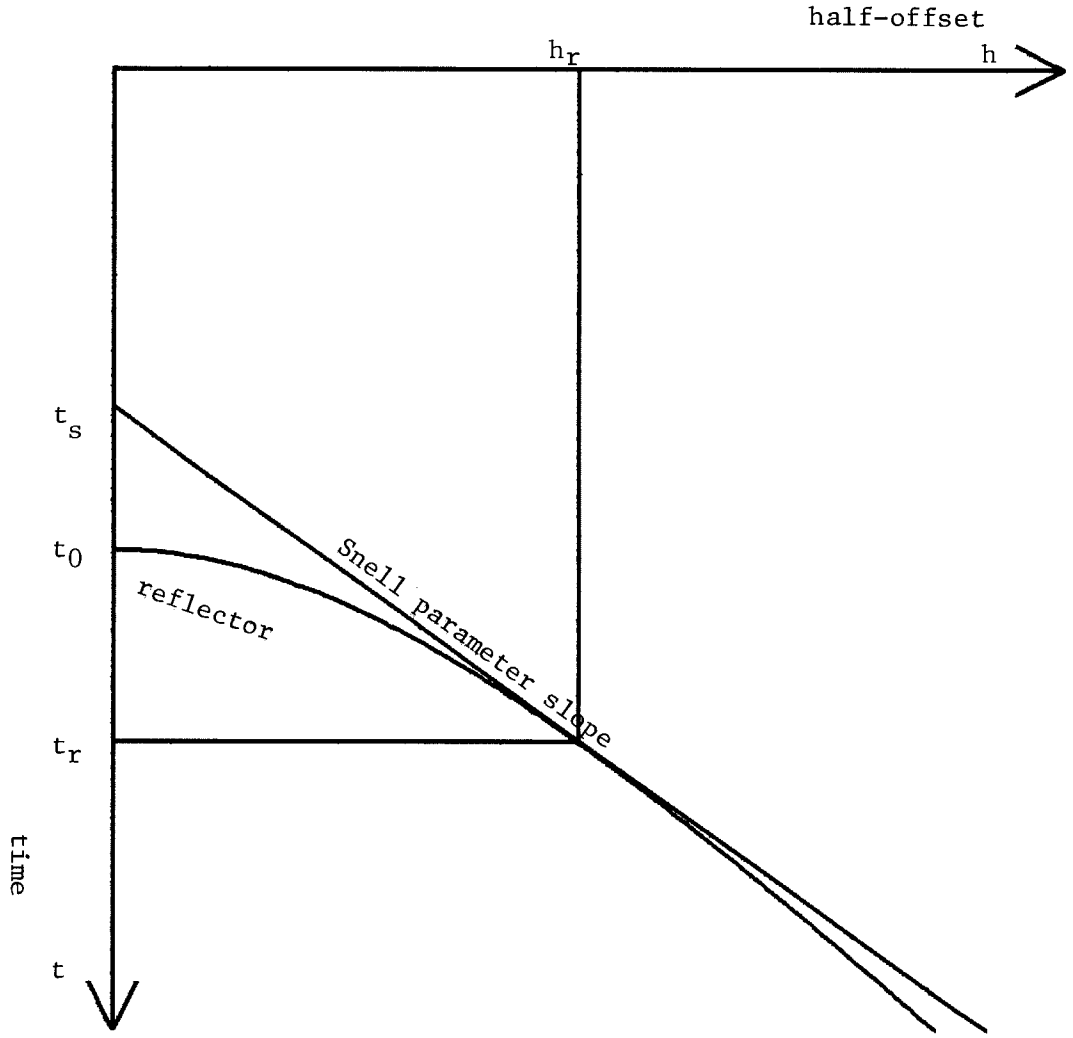

FIG. 4. Relationship between various variables used to determine the trajectory of the radial trace. The radial trace trajectory is defined as the tangency of the Snell parameter slope with the reflector curves of flat events at all depths. The reflector curve obeys equation (4) and the Snell parameter slope is given by equation (5). The time-axis-intercepts of these two curves are denoted as slant time t_s and are the slant time t_s and t_0. The coordinates of the tangency point are called radial time t_r and radial offset h_r.

where t_h is reflection time at any half-offset h. A Snell parameter line is given by

$$t_s = t_h - 2ph \tag{5}$$

The unknown t_h is eliminated from equations (4) and (5) to give

$$t_s = \left(t_0^2 + \frac{4h^2}{v^2}\right)^{\frac{1}{2}} - 2ph \tag{6}$$

The tangency point is the reflection curve maximum within a coordinate system skewed with a slope of Snell's parameter (i.e. linear moveout). Therefore, the tangency point is found by setting the derivative of t_s equal to zero:

$$\frac{\partial t_s}{\partial h} = 0 = \frac{4h}{\left(v^2 t_0^2 + 4h^2\right)^{\frac{1}{2}}} \tag{7}$$

This is then solved for $h = h_r$:

$$h_r = \frac{pv^2 t_0}{2}\left(1 - p^2v^2\right)^{-\frac{1}{2}} \tag{8}$$

Inserting equation (8) into equation (4) gives

$$t_r = t_0\left(1 - p^2v^2\right)^{-\frac{1}{2}} \tag{9}$$

Likewise, inserting into equation (6) leaves

$$t_s = t_0\left(1 - p^2v^2\right)^{\frac{1}{2}} \tag{10}$$

The radial parameter r is just the ratio of h_r to t_r:

$$r = \frac{pv^2}{2} \tag{11}$$

Since this is a constant velocity medium, r is constant, and the radial trace equation (2) is that of a straight line.

The definition of radial parameter as given by equation (11) has a couple of satisfying implications. First, inserting this definition into the diffractor description of equation (3) reduces the expression in parentheses to the familar Snell parameter cosine term

$$vt = \left[\frac{z^2}{\left(1 - p^2 v^2\right)} + y^2 \right]^{\frac{1}{2}} \tag{12}$$

This cosine-depth scaling is the same scaling as for vertical traveltime, given by equation (9). Second, equation (11) may be derived directly from frequency domain imaging theory (Claerbout, SEP-14) by equating two definitions of the normalized offset wavenumber H:

$$H = \frac{vk_h}{2\omega} = \frac{2h}{vt} = pv \tag{13}$$

and solving for h/t.

Flat Reflectors in Depth-Variable Velocity Media

The radial trace descriptions of equations (8), (9) and (10) can easily be extended to depth-variable velocity media because they have been written in terms of Snell's parameter, which is invariant over velocity variations. Vertical traveltime t_0 is replaced by an integral in each case to give

$$h_r = \frac{1}{2} \int_0^{t_0} dt_0 pv^2 \left(1 - p^2 v^2\right)^{-\frac{1}{2}} \tag{14}$$

$$t_r = \int_0^{t_0} dt_0 \left(1 - p^2 v^2\right)^{-\frac{1}{2}} \tag{15}$$

$$t_s = \int_0^{t_0} dt_0 \left(1 - p^2 v^2\right)^{\frac{1}{2}} \tag{16}$$

The root mean-squared approximation of equation (14) is very good in practice. In variable velocity media, equations (14) and (15) describe a curved line, convex timewards for increasing velocities, and concave timewards for decreasing velocities. Examples will be shown in the next section.

From the latter two equations a relationship between reflection times on slant stack and radial traces can be derived.

$$t_s = \int_0^{t_r} dt_r \left(1 - p^2 v^2\right) \tag{17}$$

Therefore, radial trace sections could be moved out using equation (17) and then migrated by the frequency domain slant stack migration operator. However, it must be remember that the equations developed so far are exact only for flat reflectors.

Examples

Radial trace sections have been constructed for the model described in figures 5 through 7. Figure 5 depicts the point scatterer locations and figure 6 the velocity model. 64 midpoint gathers with 64 offsets with the same midpoint and offset spacing, four of which are shown in figure 7, were constructed with a ray tracing program according to this model. The flat tops of the diffraction curves at wide offsets in figure 7 are predicted by the double square root equation (1). Then 64 radial gathers, four of which are shown in figure 9, were mapped from the common midpoint gathers according to the trajectories given in figure 8. Finally, the radial gathers were sorted into 64 midpoint sections of the same Snell parameter, four of which are shown in figure 11. As predicted by equation (3), the diffraction response of point scatterers on the radial trace sections in figure 11 has a hyperbolic character.

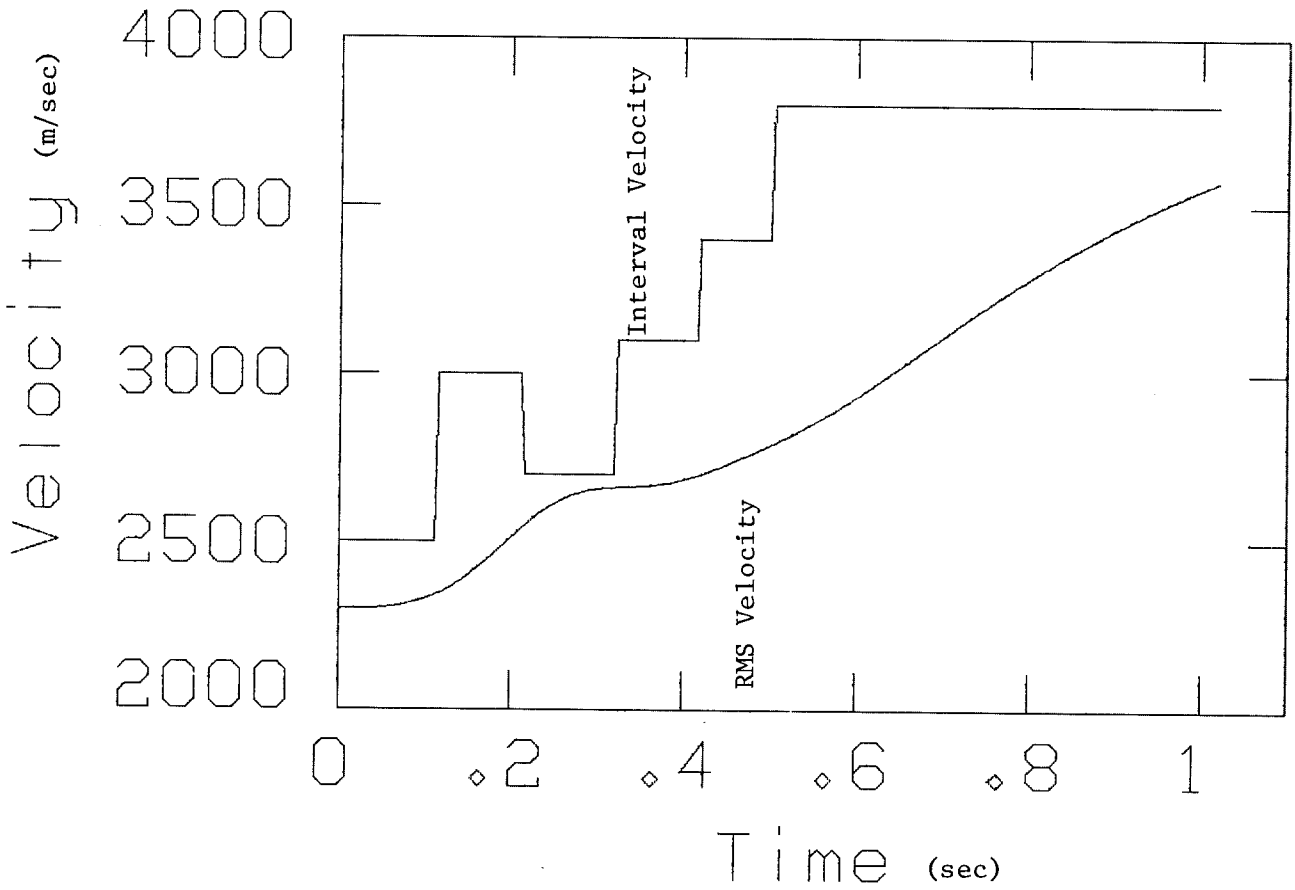

FIG. 6. The vertical traveltime interval and smoothed root-mean-squared velocity structure of the model of figure 5.

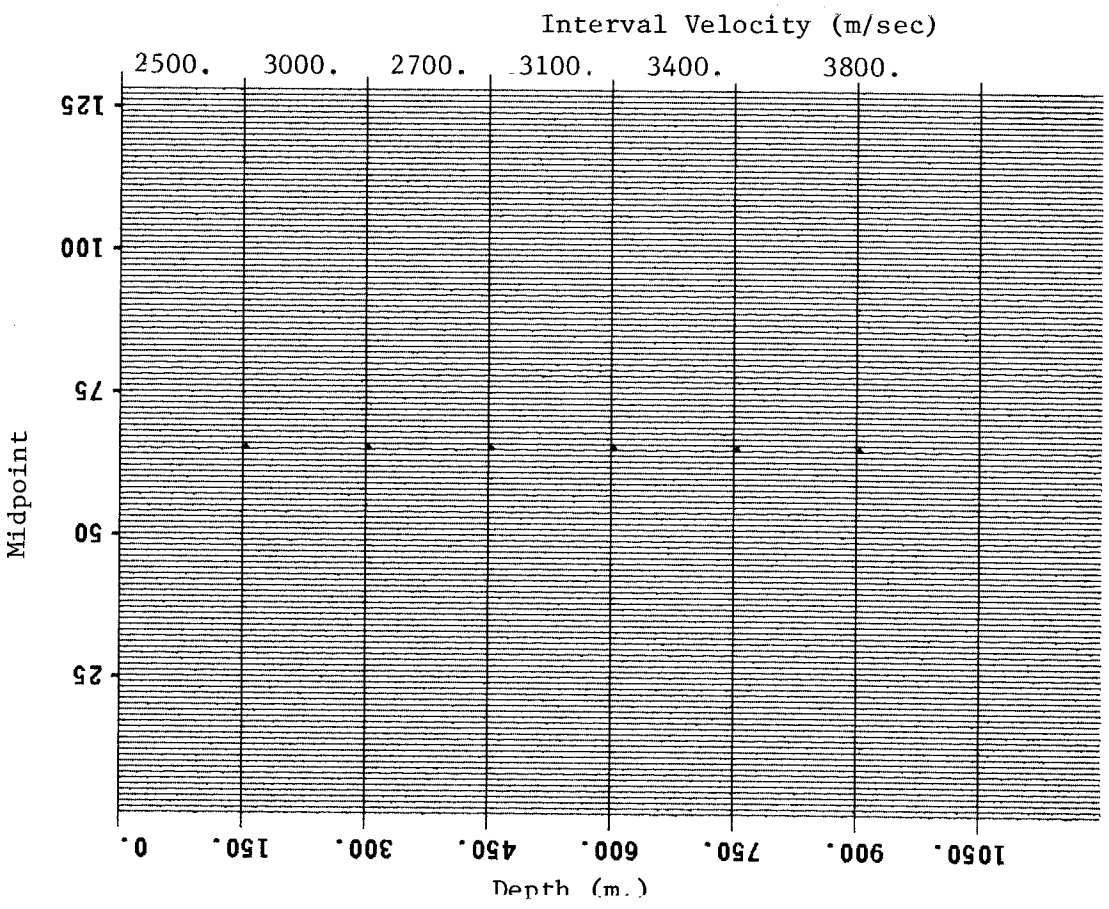

FIG. 5. The earth model used to generate constant offset diffraction curves consists of six point scatterers at the interfaces of constant velocity layers 150 m thick. The thickness and interval velocity of each layer are given on the left and right axes. This model has a low velocity zone in the third layer.

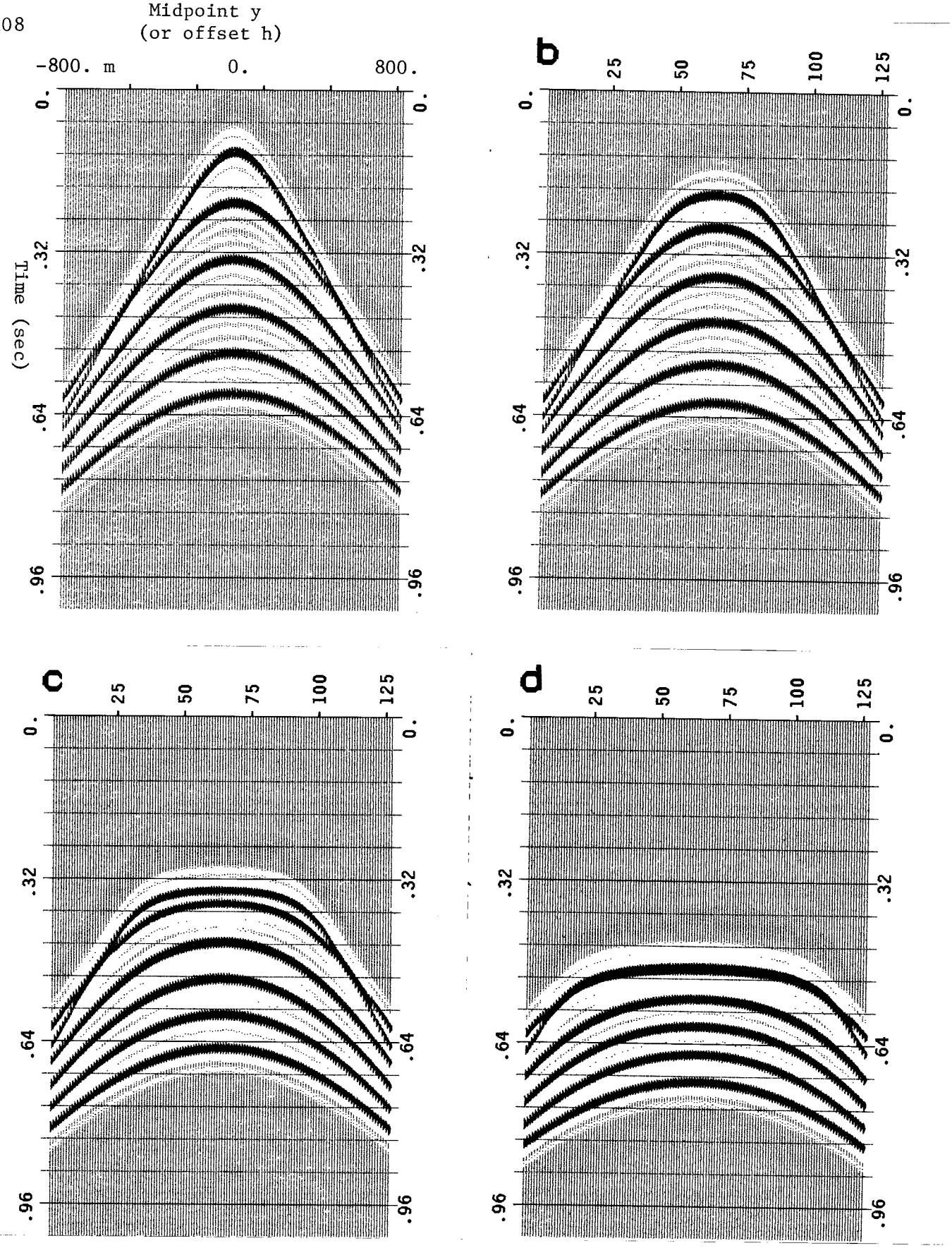

FIG. 7. Four of the 64 constant offset sections generated for the model of figure 5. Offsets are (a) 0 m, (b) 200 m, (c) 400 m, and (d) 600 m. As approximately predicted by equation (1), diffraction curves at wide offsets have flattened tops. Midpoint and offset separations were both 12.5 m. Because the offset and midpoint separations are equal, the split spread common midpoint gathers look just like the constant offset sections. See figure 1 for a geometric explanation of this fact. These common midpoint gathers would come from the following midpoints of the above constant offset sections: (a) 64, (b) 48 or 80, (c) 32 or 96, (d) 16 or 112.

The deterioration of the reflection events in figure 9 is due to three causes. First, the radial-trace-mapping trajectory runs off the edge of the common midpoint gather, thereby truncating events. The second cause is "moveout stretch" phenomena resulting from oversampling a given offset trace. On figure 8 a radial trace trajectory for a high Snell parameter has flattened out at wide offsets. Finally, a cubic spline was used to interpolate along a row of offsets at a constant time value. Such an interpolation scheme worsens when there is significant dip between offsets, such as at wide offsets and at the boundaries, or at the widest offset.

The next set of figures is an example of a radial trace section from an actual dataset. Figure 14a is a radial trace section of the Digicon Devilish growth fault dataset constructed for the radial trace trajectory of figure 12 and velocity structure of figure 13. Figure 14b is the slant stack section constructed for the same Snell parameter as for the radial trace section. As predicted by the relationships worked out earlier, the time of an event on a radial trace section is greater than the same event on a slant stack section. Figure 14c compares a portion of the radial trace section moved out to slant time to the same portion of the slant stack section. The reflection times are close to equal, though as expected, the discrepancy increases for dipping reflectors.

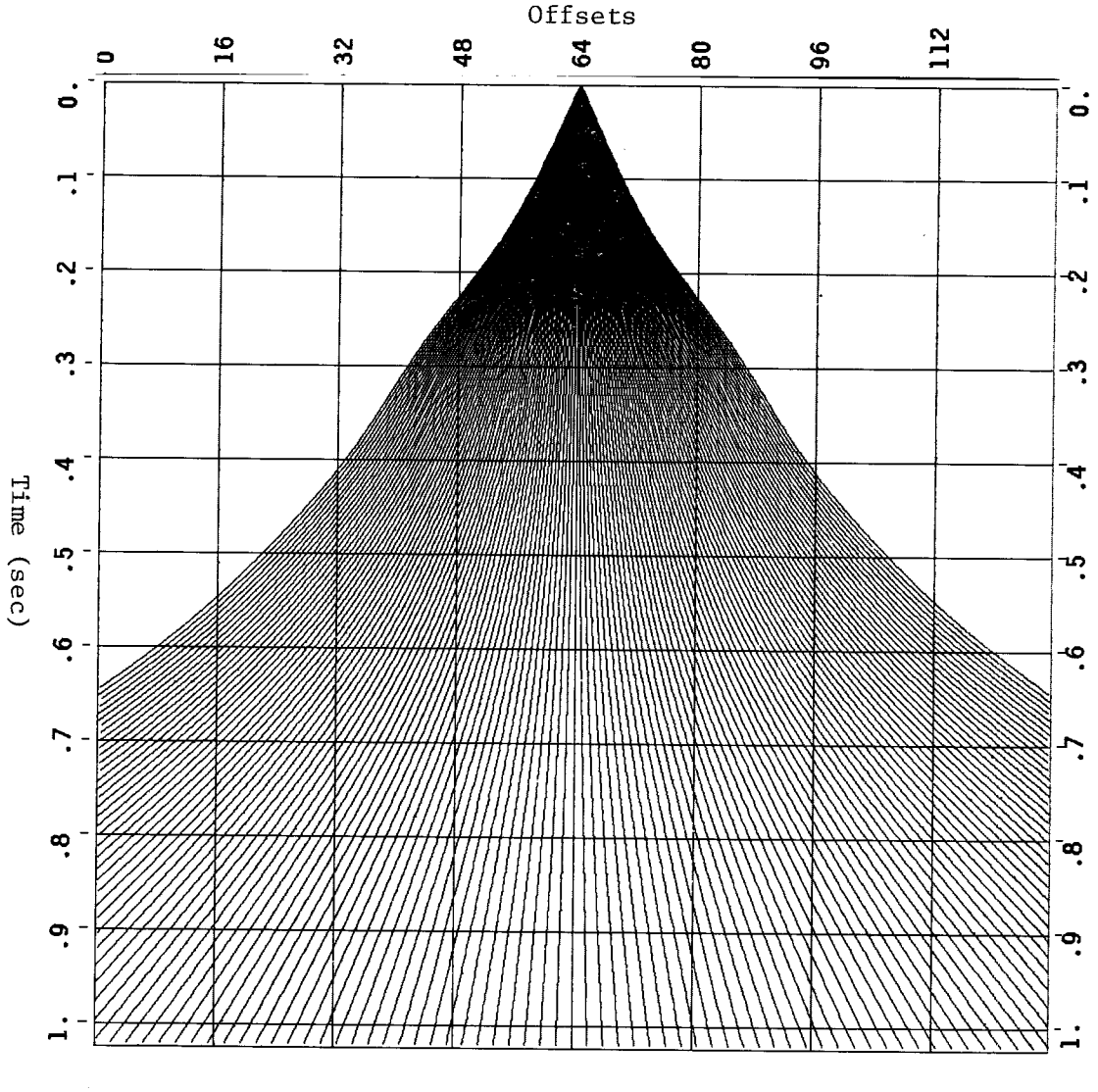

FIG. 8. Radial trace trajectories used to map the common midpoint gathers of figure 7 into the radial trace gathers of figure 9. The trace numbers correspond with those of figure 7. Snell parameter separation is 2.e-06 m/sec with maximum Snell parameter of 1.26e-04 m/sec. For a velocity structure which increases with depth, the trajectories are convex timewards. The small bump at 0.3 seconds is due to the low velocity zone.

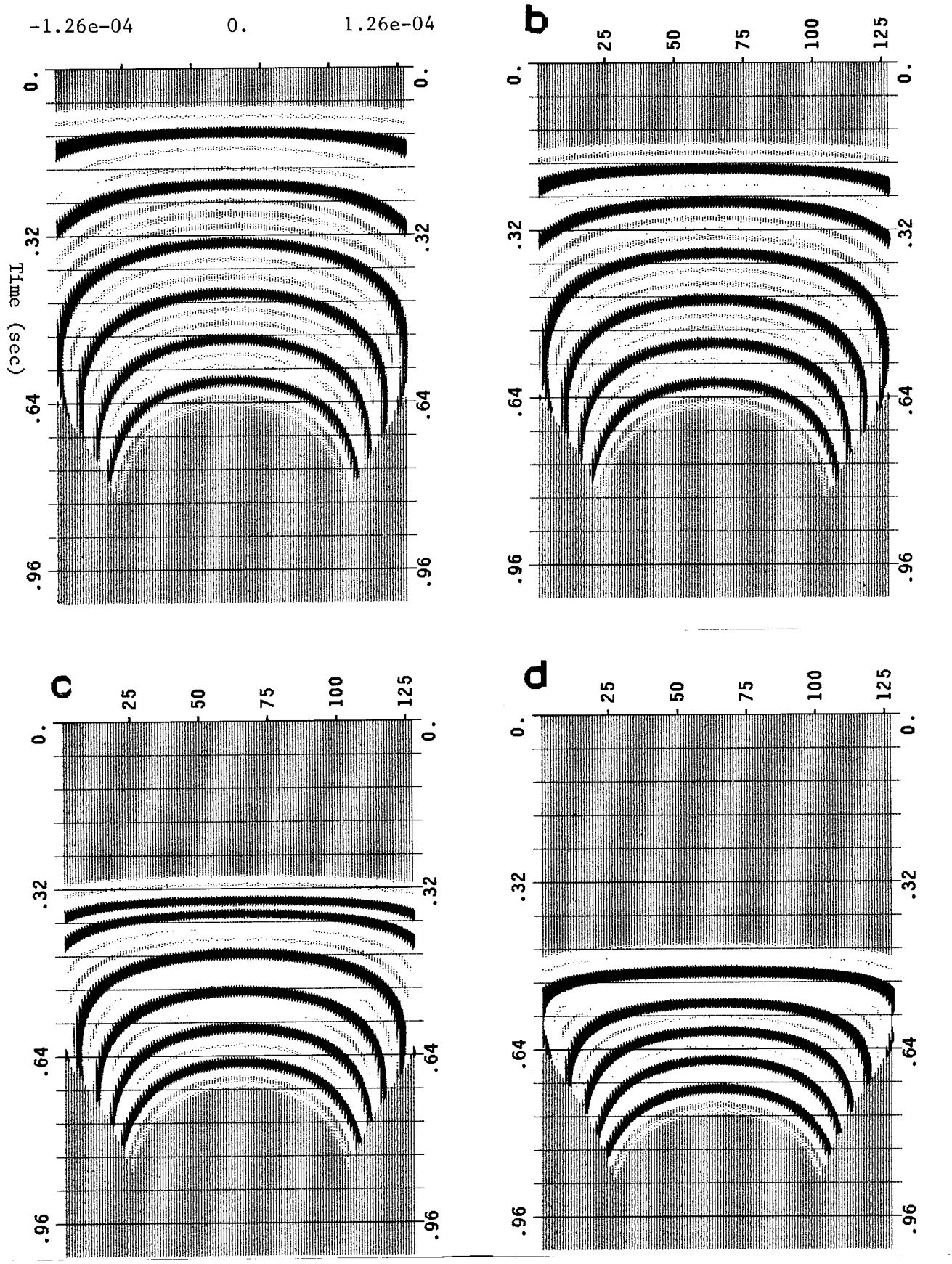

FIG. 9. The radial trace gathers generated from the common midpoint gathers of figure 7 according to the mapping described by figure 8. A ***radial trace gather*** is a collection of traces mapped for different radial parameters at the same midpoint. The Snell parameter increases from the minimum of -1.26e-04 m/sec at trace 1 to 0.0 at trace 64 and to +1.26e-4 m/sec at trace 127. The radial trace gathers common from the following midpoints of the constant offset sections of figure 8: (a) 64, (b) 48 or 80, (c) 32 or 96, (d) 16 or 112.

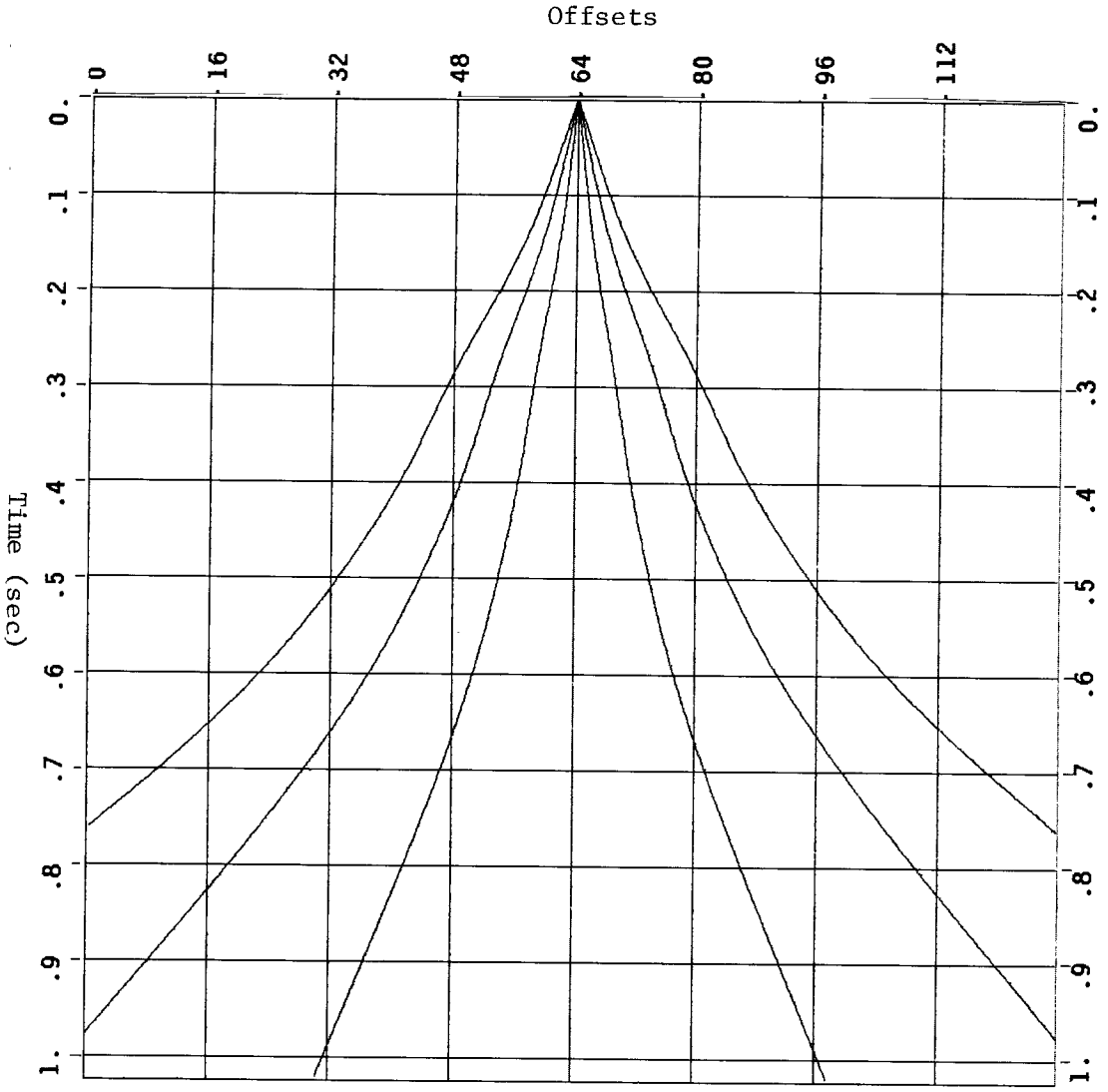

FIG. 10. The same figure as figure 8 except showing only the radial trajectories of the radial trace sections of figure 11. The Snell parameter increment is 3.2e-5 m/sec.

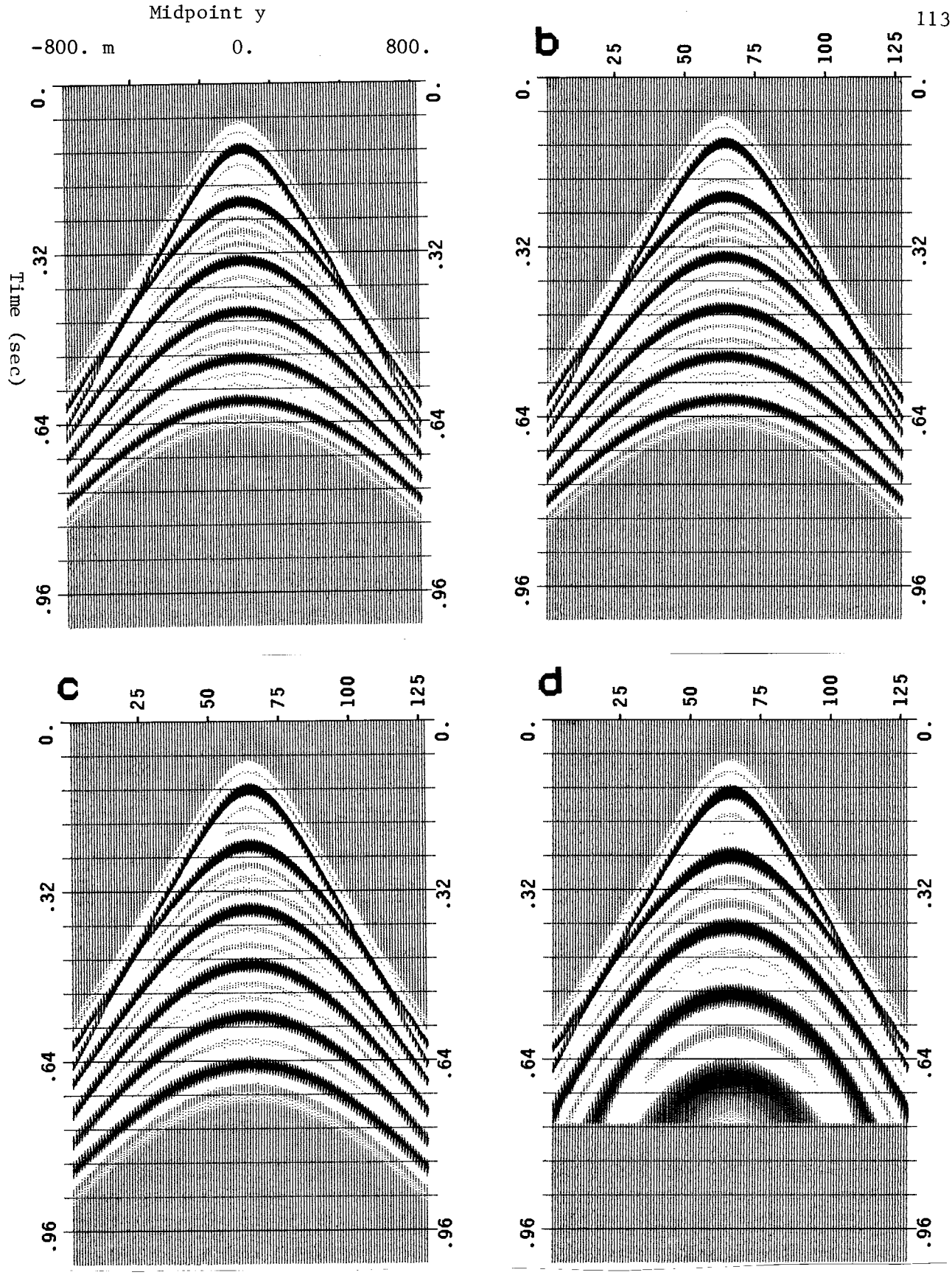

FIG. 11. Radial trace sections of the model of figure 5 made at the trajectories indicated in figure 10. A ***radial trace section*** is the set of radial traces from each midpoint mapped at the same radial parameter. The Snell parameters of each section are (a) 0. m/sec, (b) 3.2 m/sec, (c) 6.4 m/sec, and (d) 9.6 m/sec. The moveout between sections formed for different radial parameters is slight, as suggested by the radial trace gathers of figure 9. Figures (c) and (d) demonstrate the artifacts of constructing radial trace sections by using cubic spline interpolation: (1) end of gather cutoff, (2) moveout-like stretch due to oversampling offsets especially at wide offsets, and (3) interpolating dipping segments using horizontal samples.

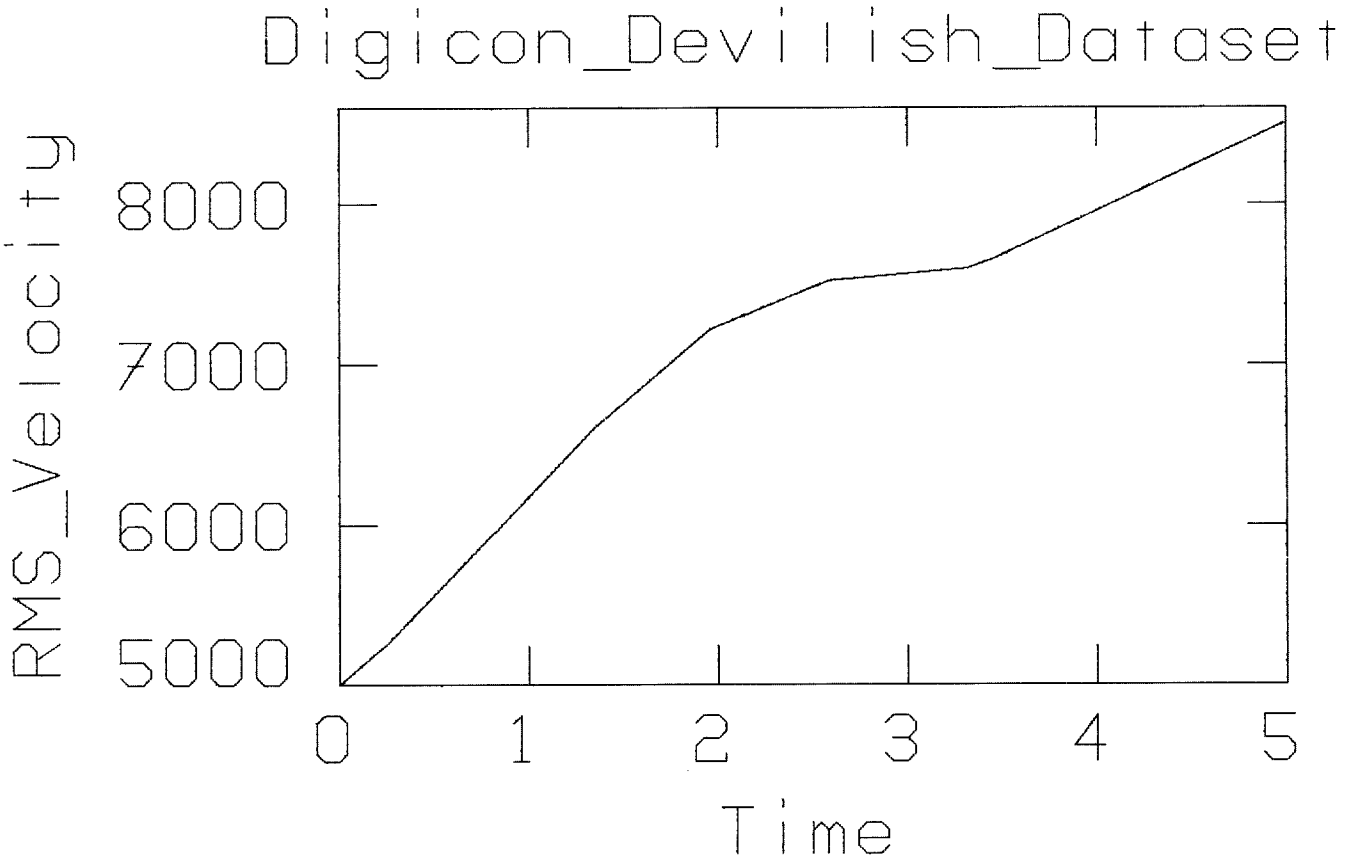

FIG. 13. RMS velocity structure of the Digicon Devilish dataset.

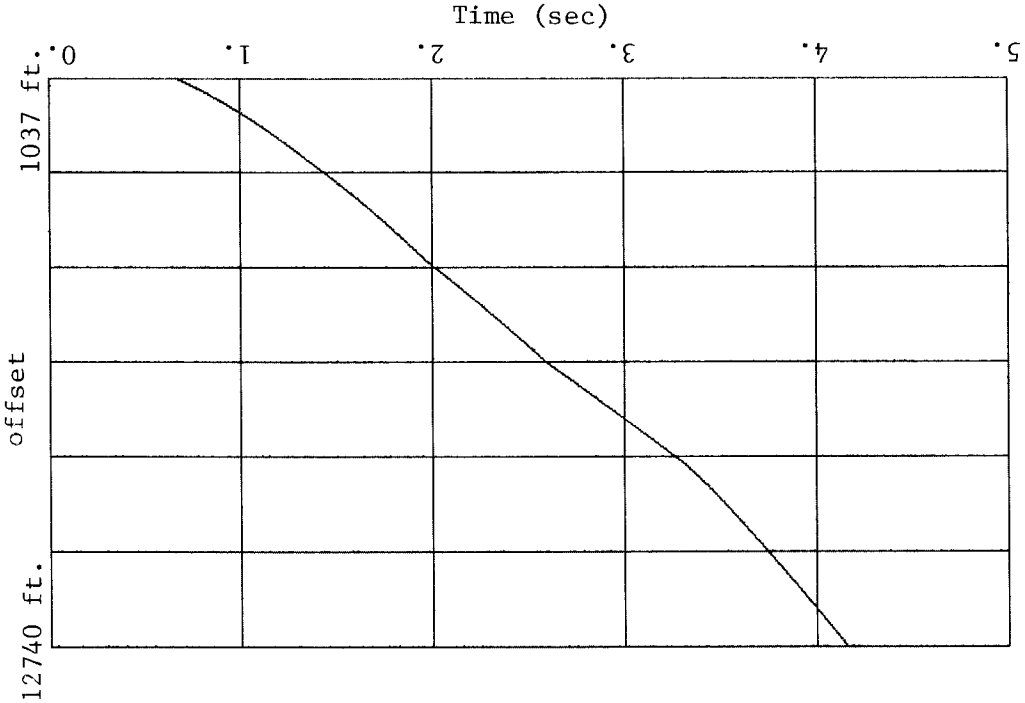

FIG. 12. The radial trace and (flat-event) slant stack trajectory used to create figure 14. The Digicon Devilish dataset is 4mil, 5 secs, 48-fold data, with a spread of 1037 to 12740 feet. The Snell parameter is 4.5e-05 feet/sec.

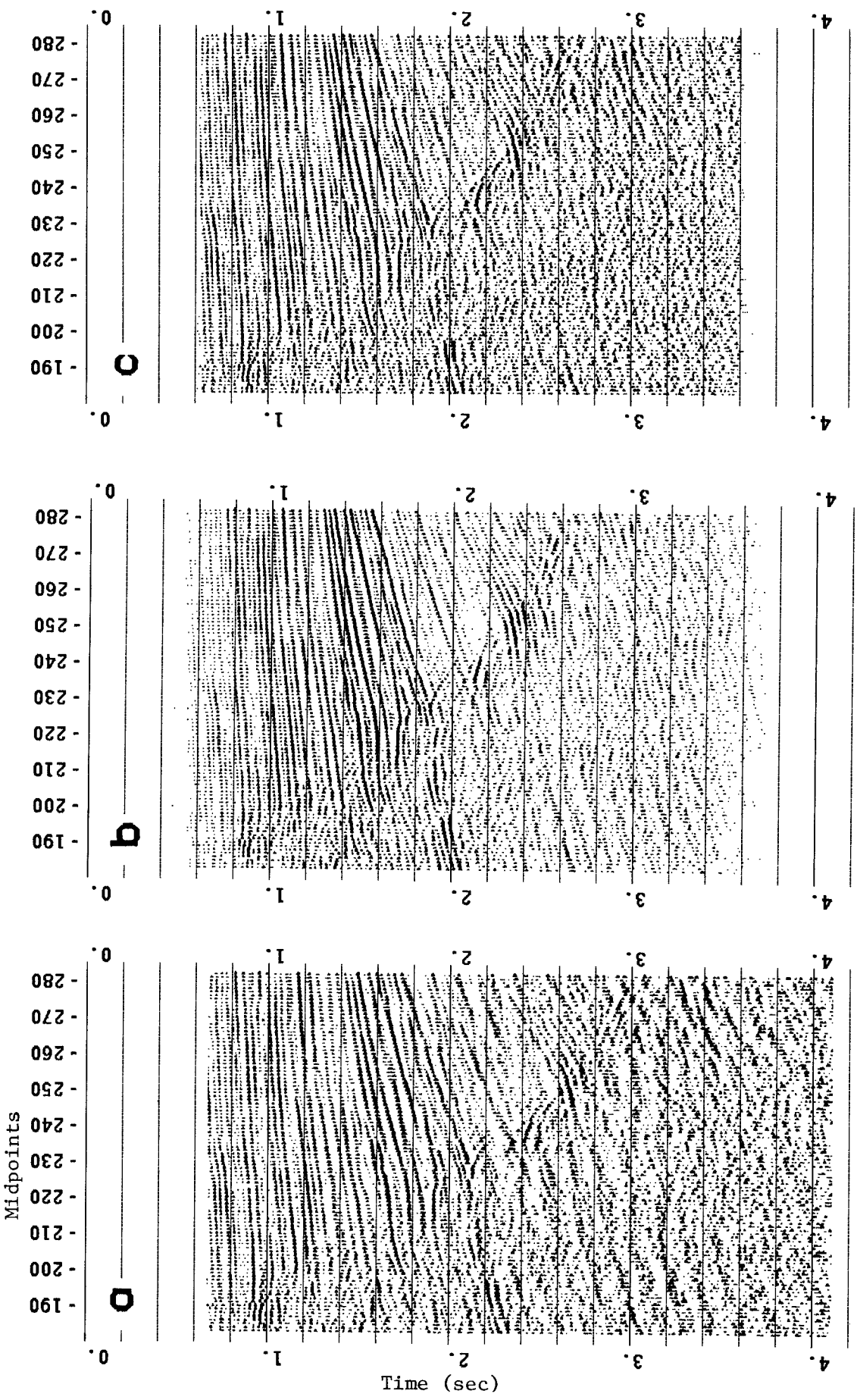

FIG. 14. Radial trace (a), slant stack (b), and radial-to-slant trace moveout (c) sections of the Digicon Devilish growth fault dataset, each created with the same Snell parameter given in figure 12. As predicted by figure 2, the radial trace times (a) are greater than those of a slant stack (b). However, applying the moveout correction of equation (18) brings the radial trace times (c) into agreement with the slant stack times (b). The greatest discrepancies between (b) and (c) are for dipping events because the moveout equation is correct only for flat events. Another difference between slant stack and radial trace sections is that because the former is a *stack* there is an improvement in the signal-to-noise. Also the non-abrupt drop-off at the top and bottom of the slant stack section is due to the fact that, in contrast to radial trace extraction, the slant stacking process continues to operate beyond the end of the offset spread unless the pre-stack data were muted as in the above case (Schultz, SEP-9).